Low Temperature Physics/Fizika Nizkikh Temperatur, 2014, v. 40, No. 4, pp. 400–404

# Fermi surface and effect of high magnetic fields on the metal–semimetal Peierls-like transition of $(TSeT)_2Cl$

Vladimir Laukhin[1,2], Alain Audouard[3], David Vignolles[3], Loïc Drigo[3], Pere Alemany[4], and Enric Canadell[2]

[1]*Institut Català de Recerca i Estudis Avançats (ICREA), Barcelona, Spain*
E-mail: vladimir@icmab.es

[2]*Institut de Ciència de Materials de Barcelona (CSIC), Campus UAB, Bellaterra 08193, Spain*

[3]*Laboratoire National des Champs Magnétiques Intenses (UPR 3228 CNRS, INSA, UJF, UPS) 143 Avenue de Rangueil, F-31400 Toulouse, France*

[4]*Departament de Química Física and Institut de Química Teòrica i Computacional (IQTCUB) Universitat de Barcelona, Martí i Franquès 1, Barcelona 08028, Spain*

Received October 18, 2013

Resistance measurements in pulsed magnetic fields up to 55 T as well as a first-principles DFT calculation of the Fermi surface for the organic metal $(TSeT)_2Cl$ have been performed to investigate its metal–semimetal phase transition. The results obtained are in line with the imperfect nesting that can be inferred from both the observed metallic behavior of the resistivity at low temperature and the previously reported Shubnikov–de Haas oscillations due to small carrier pockets. The DFT study points out the possibility that the LUMO bands of the TSeT donor may interact with the HOMO ones and modify the shape of the Fermi surface under pressure.

PACS: **71.18.+y** Fermi surface: calculations and measurements; effective mass, *g*-factor;
71.20.Rv Polymers and organic compounds;
72.15.Gd Galvanomagnetic and other magnetotransport effects.

Keywords: Fermi surface, organic metals, metal–semimetal phase transition, field-dependent resistance.

## 1. Introduction

The charge transfer salt $(TSeT)_2Cl$ (where TSeT stands for tetraselenotetracene) is one of the oldest studied organic metals [1,2]. It has a structure typical for quasi-one-dimensional organic metals with stacks of TSeT molecules extending along the *c* axis and $Cl^-$ anions in between (see Fig. 1(a)) [2]. As already reported [1,3–5], a metallic behavior is observed down to 28 K, followed by a sharp resistance increase attributed to a charge-density-wave (CDW) condensation [6]. However, in this particular case the transition only induces a partial reduction in the number of conducting carriers, so that the low-temperature state is still semimetallic with the resistivity remaining at the level of its room temperature value. As the temperature further decreases, a metallic behavior is again observed below 13 K which is the signature of an imperfect nesting. This is in agreement with the existence of small carrier pockets yielding Shubnikov–de Haas oscillations at liquid helium temperatures with frequency corresponding to 0.3% of the area of the first Brillouin zone [6–8]. Assuming that the inflexion point in the temperature dependence of the resistance corresponds to the zero-field CDW transition temperature it is possible to derive that $T_{CDW}(0) = (20.0 \pm 0.6)$ K (see inset in Fig. 2). In order to clarify the nature of this metal–semimetal transition we have studied the effect of high pulsed magnetic fields up to 55 T on the resistance of $(TSeT)_2Cl$ single crystals in the temperature range 10–28 K and carried out a first-principles theoretical study of its band structure and Fermi surface.

## 2. Experimental

Sample resistance was measured along the conducting direction, i.e., along the needle axis, with a 1 mA alternating current. Electrical contacts to the crystal were made using annealed platinum wires of 20 μm in diameter glued

© Vladimir Laukhin, Alain Audouard, David Vignolles, Loïc Drigo, Pere Alemany, and Enric Canadell, 2014

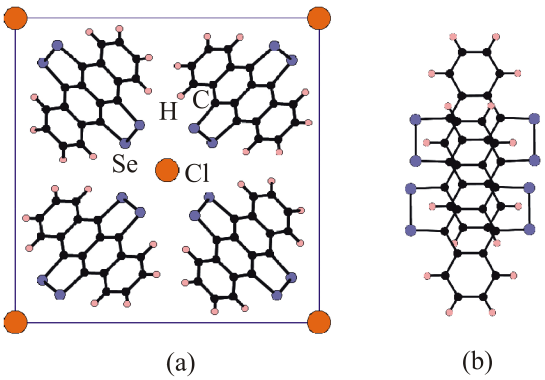


*Fig. 1.* (Color online) $(TSeT)_2Cl$: (a) view of the 293 K crystal structure along *c*, and (b) overlap mode between two TSeT donors.

with graphite paste. The frequency was either 77 Hz in zero field or 20 kHz in magnetic fields. The cooling rate was $\simeq$ 1 K/min and 0.5 K/min above and below 77 K, respectively. Transverse magnetoresistance measurements were performed up to 55 T in pulsed magnetic fields applied perpendicular to the needle axis, with a pulse decay duration of 0.36 s in the temperature range from 10 to 28 K. A lock-in amplifier with a time constant of 30 μs was used to detect the signal across the potential contacts.

### 3. Computational details

The present calculations were carried out using a numerical atomic orbitals density functional theory (DFT) approach [9,10], which was developed for efficient calculations in large systems and implemented in the SIESTA code [11–14]. We have used the generalized gradient approximation (GGA) to DFT and, in particular, the functional of Perdew, Burke and Ernzerhof [15]. Only the valence electrons are considered in the calculation, with the core being replaced by norm-conserving scalar relativistic pseudopotentials [16] factorized in the Kleinman–Bylander form [17]. We have used a split-valence double-ζ basis set including polarization orbitals with an energy shift of 10 meV for all atoms [18]. The energy cutoff of the real space integration mesh was 250 Ry. The Brillouin zone was sampled using a grid of (20×20×20) *k*-points [19]. The experimental 293 K and ambient pressure crystal structure of Le Pévelen *et al.* [20,21] was used in the calculations.

### 4. Resistance measurements

The temperature dependence of the zero-field resistance is displayed in Fig. 2. As mentioned above, a metallic behavior is observed down to 28 K, followed by a sharp resistance increase possibly due to a charge-density-wave condensation [6]. When lowering the temperature a metallic behavior is again observed below 13 K. A zero-field CDW transition temperature $T_{CDW}(0) = (20.0 \pm 0.6)$ K can be evaluated from the inset in Fig. 2 assuming that the

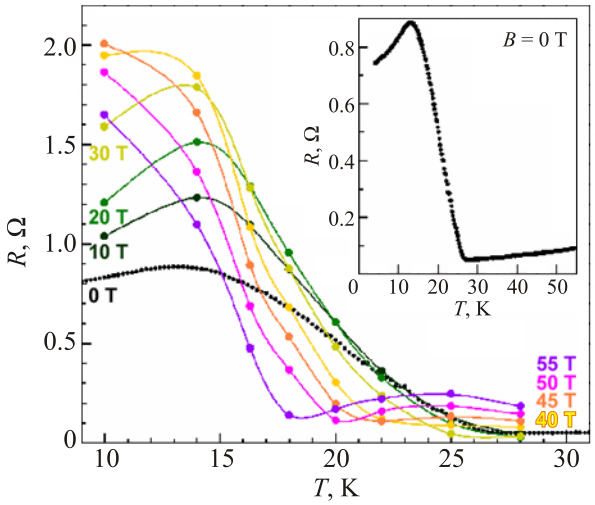


*Fig. 2.* (Color online) Temperature dependence of the resistance for various values of the magnetic field. The inset displays the data in zero field for a larger temperature range.

inflexion point is associated with the onset of the CDW state.

In the temperature range 10–28 K, the field-dependent resistance displayed in Fig. 3, is strongly non-monotonic. In particular, a bump is observed suggesting a field-induced metallic state. This bump is indeed followed by a minimum for the data collected in the temperature range between 18 and 28 K and afterwards the resistance increases again.

The temperature dependence of the resistance at a given magnetic field can be derived from this magnetoresistance data, as reported in Fig. 2 (main panel). The sharp resistance increase observed as the temperature decreases in zero field, attributed to the CDW condensation, is also observed in magnetic field albeit at lower temperatures. The field dependence of $T_{CDW}$ can be derived from these data, as displayed in Fig. 4, which evidences that $T_{CDW}$ de-

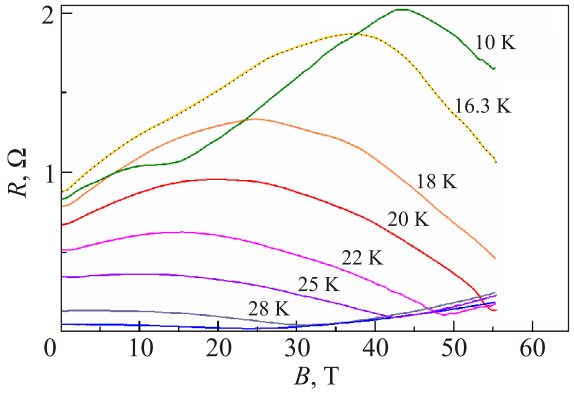


*Fig. 3.* (Color online) Field-dependent resistance at various temperatures.

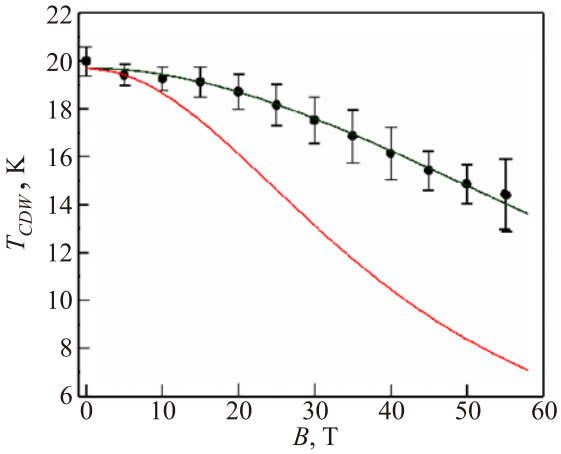


*Fig. 4.* (Color online) Field dependence of $T_{CDW}$ deduced from the data in Fig. 2 (solid circles). Red solid line is obtained from Eq. (1) with $T_{CDW}(0)$ = 19.7 K. Black solid line is the best fit of Eq. (2) with $T_{CDW}(0)$ = 19.7 K and $T^*$ = 40.3 K.

creases as the magnetic field increases. Similar behavior has been already observed, e.g., for the perylene compound (Perylene)$_2$[Pt(S$_2$C$_2$(CN)$_2$)$_2$] ($T_{CDW}(0)$ = 8.4 K) [22] and attributed to the Pauli effect, i.e., the field-induced Zeeman splitting, which decreases $T_{CDW}$ according to the equation

$$\ln\frac{T_{CDW}(0)}{T_{CDW}} = \mathrm{Re}\left[\Psi\left(\frac{1}{2}+i\frac{\mu_B B}{2\pi k_B T_{CDW}}\right)\right]-\Psi\left(\frac{1}{2}\right), \quad (1)$$

where $\Psi$ is the digamma function. As displayed in Fig. 4, Eq. (1) cannot hold for the data that are much less sensitive to the magnetic field strength than predicted. Indeed, in the case of imperfect nesting, the orbital effect which increases the one-dimensionality of the electronic system, hence $T_{CDW}$, must be taken into account. As reported in the case of the above cited perylene compound [23,24] the field dependence of $T_{CDW}$ can be accounted for by introducing a temperature $T^*$ higher than the actual $T_{CDW}$ value in the right hand side of Eq. (1). In other words, Eq. (1) should be modified as

$$\ln\frac{T_{CDW}(0)}{T_{CDW}} = \mathrm{Re}\left[\Psi\left(\frac{1}{2}+i\frac{\mu_B B}{2\pi k_B T^*}\right)\right]-\Psi\left(\frac{1}{2}\right). \quad (2)$$

In the case of (TSeT)$_2$Cl, the best fit of Eq. (2) is obtained with $T^*$ = (40 ± 4) K which is substantially higher than $T_{CDW}(0)$, indicating that the orbital effect must be taken into account.

### 5. Band structure and Fermi surface

As mentioned, the 293 K crystal structure of (TSeT)$_2$Cl is tetragonal $P4_2/n$ and contains four parallel chains of TSeT donors per unit cell (see Fig. 1(a)). Successive donors of a chain are longitudinally slipped leading to the intermolecular overlap shown in Fig. 1(b). There are numerous C...C contacts with length in between 3.372 and 3.562 Å as well as Se...Se contacts of 3.481 Å associated with this overlap insuring a good interaction of the highest occupied molecular orbitals (HOMO)s of successive donors along the chain. In contrast, there are no C...C contacts and only a considerably longer Se...Se contact of 3.799 Å between donors of different chains. Consequently, (TSeT)$_2$Cl is expected to be a strongly one-dimensional (1D) compound.

The calculated band structure along several directions of the tetragonal Brillouin zone is shown in Fig. 5. The four partially filled bands in this figure are built from the HOMO of TSeT, which is a π-type orbital with large contribution from the $p_z$ orbital of all of the carbon atoms and a smaller one from that of the selenium atoms. These bands are strongly dispersive (∼ 1 eV) along the $c^*$ direction whereas they exhibit a small or nil dispersion along the transverse directions. Because of the stoichiometry there are six electrons to fill these bands so that in average the bands are 3/4 filled. Thus, the present first-principles calculations confirm that (TSeT)$_2$Cl is a strongly 1D metal.

The calculated Fermi surface is shown in Fig. 6. It is made of two sets of four slightly undulating sheets perpendicular to the $c^*$ direction. These sheets occur on a relatively narrow region of the Brillouin zone, in between two planes perpendicular to the $c^*$ direction at 0.35$c^*$ and 0.40$c^*$ (and at –0.35$c^*$ and –0.40$c^*$). Two of these sheets touch at some points of the Brillouin zone. Essentially, these sheets can be described as originating from the interaction and hybridization of two almost completely flat sheets (i.e., those associated with the two superposed bands in the $\Gamma \to Z$ direction of Fig. 5 which exhibit a nil dispersion along the $\Gamma \to X$ direction) in-between an upper and a

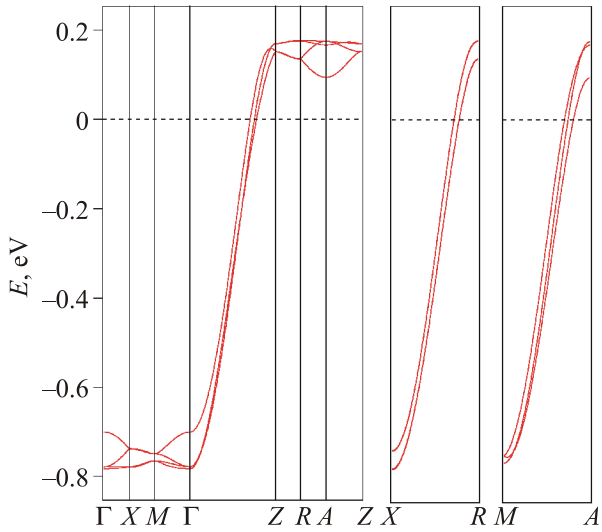


*Fig. 5.* (Color online) DFT band structure for the 293 K crystal structure of (TSeT)$_2$Cl. The dashed line refers to the Fermi level. Γ :(0,0,0), *X*: (1/2,0,0), *M*: (1/2,1/2,0), *Z*: (0,0,1/2), *R*: (1/2,0,1/2) and *A*: (1/2,1/2,1/2) in units of the tetragonal reciprocal lattice vectors.

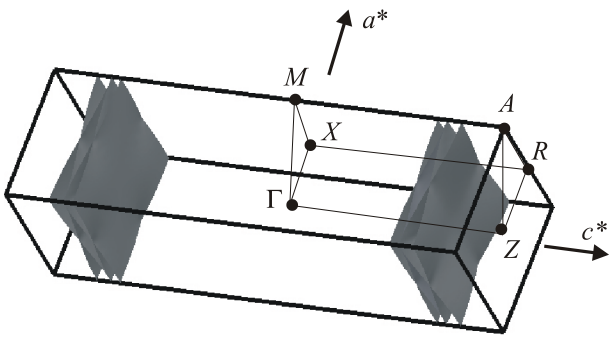


*Fig. 6.* DFT Fermi surface for the 293 K crystal structure of $(TSeT)_2Cl$.

lower sheets (i.e., those associated with the right and left bands around the previous ones in the $\Gamma \to Z$ direction of Fig. 5 which exhibit a non-nil dispersion along the $\Gamma \to X$ direction) that are more warped. As a result of the interaction, inside the Brillouin zone all sheets acquire warping and lead to the Fermi surfaces of Fig. 6. The separation between the upper and lower pair of sheets in that figure is not the same (see for instance the separation between the four bands along the $\Gamma \to Z$ direction when they cut the Fermi level in Fig. 5). Thus, a common nesting vector cannot destroy completely the four sheets of the Fermi surface. A nesting vector $q = 0.75c^*$ connects large parts of the four sheets and thus must be responsible for the sharp resistivity increase around 28 K as well as the pretransitional fluctuations and sharp satellite reflections observed below 200 and 26 K, respectively [6]. However the nesting being not complete, pockets of carriers will remain below the Peierls-like transition and must be at the origin of the occurrence of Shubnikov–de Haas oscillations.

Note the similarity with the case of the already mentioned $(Perylene)_2[M(S_2C_2(CN)_2)_2]$ (M: Pt, Ni, Cu,...) salts which also exhibit a Fermi surface made of four slightly undulating sheets perpendicular to the perylene chains direction [25]. However, in that case the crystal structure is monoclinic and the four sheets occur as two pairs of slightly separated sheets. Although the small differences in the warping of the sheets are not relevant at high temperature, they must be the origin of the different behavior of the two salts at very low temperatures.

It is also worth noting that a second series of four bands lies only $\sim 0.25$ eV higher than the top of the HOMO bands. This feature was also noticed in an extended Hückel study of the electronic structure of this material [26,27]. These bands are built from the lowest unoccupied molecular orbits (LUMO) of TSeT which is a π-type orbital with large contribution from the $p_z$ orbital of the four selenium atoms and a smaller one from those of the carbon atoms. Because of this fact, these bands are considerably less dispersive along $c^*$. This observation raises the interesting possibility that under the influence of thermal contraction and/or pressure the two sets of bands can interact and hybridize. If the interaction is strong enough to affect the region of the Fermi level, the Fermi surface may be noticeably perturbed.

## 6. Concluding remarks

The CDW state observed below $T_{CDW}(0) = 20$ K is destabilized by Pauli effect at high magnetic field. However, in addition to this Pauli effect, the orbital effect must be taken into account to explain the field dependence of the CDW condensation temperature. This result is in line with the imperfect nesting that can be inferred from the accurate DFT Fermi surface, the observed metallic behavior of the resistivity at low temperature and the previously reported Shubnikov–de Haas oscillations due to small carrier pockets. The 293 K band structure of this solid reveals the occurrence of a group of four bands originating from the LUMO of TSeT lying only $\sim 0.25$ eV higher than the top of the HOMO bands. Thus, it is speculated that under pressure these bands could interact with the top of the partially filled HOMO bands and modify the Fermi surface, a feature probably related to the occurrence of the first order phase transition under 5 kbar leading to a new metallic phase stable down to $T < 1.3$ K [28,29].

## Acknowledgments

C.W. Mayer and B. Hilti are thanked for providing crystals of $(TSeT)_2Cl$ around twenty years ago which have been used in our measurements. We are grateful to M.-L. Doublet for communication of results. This work was supported by DGI-Spain (Grants Nos. CSD2007-00041, FIS2012-37549-C05-05 and CTQ2011-23862-C02-02), Generalitat de Catalunya (2009 SGR 1459) and XRQTC. Part of this work has been supported by EuroMagNET II under EU contract number 228043.

1. S.P. Zolotukhin, V.F. Kaminskii, A.I. Kotov, R.B. Lyubovskii, M.L. Khidekel', R.P. Shibaeva, I.F. Schegolev, and E.B. Yagubskii, *Pis'ma Zh. Exp. Teor. Fiz*. **25**, 480 (1977).
2. R.P. Shibaeva and V.F. Kaminskii, *Sov. Phys. Kristallogr.* **23**, 1183 (1978).
3. P.A. Kononovich, V.N. Laukhin, S.I. Pesotskii, I.F. Schegolev, and A.G. Khomento, *JETP Lett.* **37**, 92 (1983).
4. I.F. Schegolev and E.B. Yagubskii, in: *Extended Linear Chain Compound*s, J.S. Miller (ed.), Plenum Press, New York (1982), vol. 2, p. 385.
5. B. Hilti, C.W. Mayer, E. Minder, K. Hauenstein, J. Pfeiffer, and M. Rudin, *Chimia* **40**, 56 (1986).
6. F. Goze, A. Audouard, L. Brossard, V.N. Laukhin, J.P. Ulmet, M.L. Doublet, E. Canadell, J.P. Pouget, V.E. Zavodnik, R.P. Shibaeva, B. Hilti, and C.W. Mayer, *Synth. Met.* **70**, 1279 (1995).

7. I.F. Schegolev, P.A. Kononovich, M.V. Kartsovnik, V.N. Laukhin, S.I. Pesotskii, B. Hilti, and C.W. Mayer, *Synth. Met.* **35**, 357 (1990).
8. F. Goze, A. Audouard, L. Brossard, V.N. Laukhin, J.P. Ulmet, M.L. Doublet, E. Canadell, J.P. Pouget, V.E. Zavodnik, R.P. Shibaeva, B. Hilti, and C.W. Mayer, *Physica B* **211**, 286 (1995).
9. P. Hohenberg and W. Kohn, *Phys. Rev. B* **136**, 864 (1964).
10. W. Kohn and L.J. Sham, *Phys. Rev. A* **140**, 1133 (1965).
11. J.M. Soler, E. Artacho, J. Gale, A. García, J. Junquera, P. Ordejón, and D. Sánchez-Portal, *J. Phys.: Condens. Matter* **14**, 2745 (2002).
12. E. Artacho, E. Anglada, O. Dieguez, J.D. Gale, A. García, J. Junquera, R.M. Martin, P. Ordejón, J.M. Pruneda, D. Sánchez-Portal, and J.M. Soler, *J. Phys.: Condens. Matter* **20**, 064208 (2008).
13. For more information on the SIESTA code visit: *http://www.icmab.es/siesta/*.
14. For a review on applications of the SIESTA approach in materials science, see: D. Sánchez-Portal, P. Ordejón, and E. Canadell, *Struct. Bonding (Berlin)* **113**, 103 (2004).
15. J.P. Perdew, K. Burke, and M. Ernzerhof, *Phys. Rev. Lett.* **77**, 3865 (1996).
16. N. Troullier and J.L. Martins, *Phys. Rev. B* **43**, 1993 (1991).
17. L. Kleinman and D.M. Bylander, *Phys. Rev. Lett.* **48**, 1425 (1982).
18. E. Artacho, D. Sánchez-Portal, P. Ordejón, A. García, and J.M. Soler, *Phys. Status Solidi* (b) **215**, 809 (1999).
19. H.J. Monkhorst and J.D. Pack, *Phys. Rev. B* **13**, 5188 (1976).
20. D. Le Pévelen, *PhD Thesis*, Université de Bordeaux I (1999).
21. D. Le Pévelen, J. Gaultier, Y. Barrans, and D. Chasseau, *Synth. Met.* **103**, 2183 (1999).
22. S. Allen, J.-C. Piéri, C. Bourbonnais, M. Poirier, M. Matos, and R.T. Henriques, *Europhys. Lett.* **32**, 663 (1995).
23. G. Bonfait, M.J. Matos, R.T. Henriques, and M. Almeida, *Physica B* **211**, 297 (1995).
24. G. Bonfait and M. Almeida, *Europhys. Lett.* **36**, 477 (1996).
25. E. Canadell, M. Almeida, and J. Brooks, *Eur. Phys. J. B* **42**, 453 (2004).
26. F. Granier, *PhD Thesis*, Université de Montpellier II (2000).
27. F. Granier and M.-L. Doublet, *unpublished results*.
28. V.N. Laukhin, A.I. Kotov, M.L. Khidekel', I.F. Schegolev, and E.B. Yagubskii, *JETP Lett.* **28**, 260 (1979).
29. V.N. Laukhin and I.F. Schegolev, *JETP* **51**, 1170 (1980).